Ab Initio Study on the Mechanism of Tropospheric Reactions of the Nitrate Radical with Alkenes: Propene

M. Pilar Pérez-Casany, Ignacio Nebot-Gil,* and José Sánchez-Marín

Departament de Química Física, Facultat de Química, Universitat de València, c/Dr. Moliner, 50, 46100 Burjassot (València), Spain

Received: January 7, 2000; In Final Form: April 25, 2000

A mechanism for the reaction of the NO_3 radical with propene is proposed on the basis of B3LYP and CASSCF calculations. The mechanism involves initially both Markownikoff and contra-Markownikoff oriented addition on the double bond. From the initial radical adducts several interconnected pathways have been found, giving 1,2-epoxypropane, propanal, propenol, propanone, formaldehyde, ethanal, NO, and NO_2. The geometries of the stationary points found on the potential energy hypersurface (PES) were obtained and characterized by means of density functional theory (DFT) B3LYP/6-31G* calculations. Comparison of the optimized geometries on a limited number of molecular structures was carried out with calculations at the CASSCF level of theory with the same basis set, building the active space with five electrons in six orbitals.

1. Introduction

The reactions of the nitrate radical with unsaturated hydrocarbons represent a significant path for the loss of these compounds in the troposphere.[1] Mechanistic studies on these reactions have a double value. On one hand, they can bring some insight on and be validated by model experimental studies on simple reactions, which give only global rate constants and activation energies, such as studies on the reaction between NO_3 and propene.[2] On the other hand, the analysis of the whole reaction mechanism allows the prediction of some elementary reactions involved in the real atmosphere, since many of the proposed intermediates will react with compounds present in it, mainly oxygen molecules.

Kinetic and product data show[1] that reactions of NO_3 with alkenes proceed initially via electrophilic addition of NO_3 to the carbon−carbon double bond, forming a radical adduct intermediate, as shown in Scheme 1.

Also, it has been shown[1] that the reactions between the nitrate radical and alkenes are relatively fast, with reaction rate constants increasing as the alkyl substitution increases.[3]

Reaction products were first analyzed by means of FT-IR spectroscopy by Morris et al.[4] and Japar et al.[5] From experiments in a smog chamber under aerobic conditions, Bandow et al.[6] found that the main products are carbonyl compounds, dinitroxides, nitroxy carbonyls, and nitroxy alcohols. They made the pioneering proposal of a reaction mechanism which involves the formation of oxirane, although they did not detect it.

Wille et al.[7,8] identified the formation of oxirane at low pressures with a fast flow system and molecular beam sampling and proposed a reaction mechanism where the oxirane is the main product, although the existence of other secondary pathways in which carbonyl compounds are formed as well are not neglected.

Benter et al.[9] found a dependency of the oxirane concentration with the pressure and nature of the carrier gas. Using higher pressures and greater oxygen concentrations in the carrier gas, the formation of peroxy nitrates increased. However, under 1 bar, the oxirane yield was 75% in argon and 20% in air. A reaction mechanism in two steps was proposed. In the first one, the oxirane is formed, and in the second one, peroxy nitrates are formed in the presence of oxygen.

SCHEME 1: Formation of a Radical Adduct Intermediate

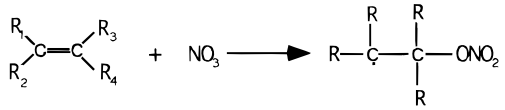

Berndt et al.,[10,11] using a low flow system, studied the reaction of the NO_3 radical with several acyclic monoalkenes in synthetic air under a pressure of 1 bar. A reaction mechanism was suggested where a direct path going from the adduct to the oxirane formation is included. A path where the adduct is collisionally deactivated was also suggested. Hence, the reaction rate of this path is favored by increasing the pressure. Then, the final products would be oxirane, carbonyl compounds, or, through oxygen addition, peroxy nitrates, ketones, and the HO_2 radical.

In a previous paper,[12] a theoretical study of the addition reaction mechanism of the NO_3 radical to the simplest alkene, ethene, was presented. In the proposed mechanism oxirane, ethanal, and nitric acid were found as main products; oxirane is the kinetically most favored product.

This work provides information on the overall mechanism in order to ascertain the main products and the energy barriers involved. We provide a theoretical explanation of the dependence of the rate constant on the substitution degree of the double bond, to complement model experimental kinetic studies. The knowledge of all the intermediates, allowing us to predict those where oxygen or other molecules such as NO_2, NO_3, and SO_2 could attack, giving other pollutant products, is another reason to analyze the complete NO_3 addition pathways.

In this work, we present a theoretical study of the mechanism of the reaction between the nitrate radical and the propene molecule. The study has been carried out in two steps. First, geometries of the stationary points were fully optimized at the B3LYP/6-31G* level. Then, single-point energy calculations using these geometries were made at the CASSCF/6-31G* level.

10.1021/jp0001034 CCC: $19.00
Published on Web 06/10/2000

SCHEME 2: Description of the Entire Reaction Mechanism

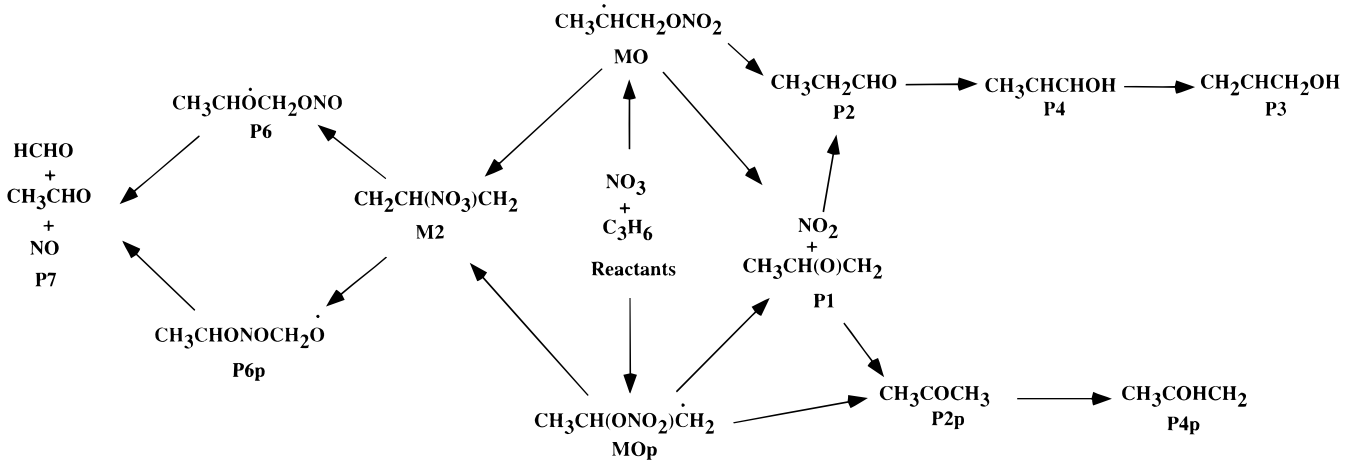

In section 2 we detail the computational aspects. In section 3 we present the results obtained; in section 3.1 a reaction mechanism is proposed and discussed, in section 3.2 a comparison is made between B3LYP geometries and CASSCF fully optimized geometries, and in section 3.3 the reaction energy profiles and the energy barrier heights involved for all the studied reaction pathways are compared. Conclusions are enumerated in section 4.

2. Computational Details

A semiempirical study, AM1,[13] of the complete potential energy hypersurface (PES) has been performed, and the stationary points have been classified according to their significance for this reaction. The AM1 results have not been included in the Results. The AM1-optimized geometries of all the relevant stationary points have been taken as starting points for a further full optimization at the density functional theory ab initio level, using the B3LYP functional. This functional is based on Becke's three-parametrization adiabatic connection method (ACM) and consists of a combination of the Slater,[14] Hartree−Fock,[15] and Becke[16] exchange functional, the Vosko, Wilk, and Nusair (VWN) local correlation functional,[17] and the Lee, Yang, and Parr (LYP) nonlocal correlation functional.[18]

The stationary points, fully optimized at the DFT level, were characterized as minima (number of imaginary frequencies NIMAG = 0), transition states (NIMAG = 1), or higher order top (NIMAG > 1) by building and diagonalizing the Hessian matrix and then analyzing the obtained normal modes by analytical methods. The eigenfollowing and transition state[19] methods have been used for the minima and transition state geometry optimizations, respectively. Some stationary points were fully optimized at the CASSCF level, to compare the calculated B3LYP and CASSCF geometries.

At the B3LYP level the Berny analytical gradient[20] was used for the minima and transition state geometry optimizations. We have used the 6-31G* basis set,[21,22] which includes polarization functions of d type on non-hydrogen atoms. Additional diffuse functions lead to convergence problems. The same basis set was used in the CASSCF optimizations.

For the CASSCF energy calculations, the active space in each point was chosen by selecting those SDCI (singles and doubles configuration interaction) natural orbitals with occupation numbers between 0.02 and 1.98.[23] The resulting active space includes seven electrons in seven orbitals for all the cases. These calculations will be thereafter denoted as CASSCF(7,7)/6-31G*. In CASSCF optimizations, the active space was reduced to five electrons in six orbitals, which will be denoted as CASSCF(5,6)/6-31G*.

CASSCF(7,7)/6-31G* energy calculations were performed by means of the MOLCAS-3 program[24] and B3LYP/6-31G* calculations and CASSCF(5,6)/6-31G* geometry optimizations with the GAUSSIAN-94 series of programs.[25]

The calculations were performed on two IBM RS6000-590 computers and an IBM SP2 computer of the Theoretical Chemistry Group of the University of València.

3. Results and Discussion

3.1. Mechanism of the Reaction. A reaction mechanism is proposed for the reaction of NO_3 with propene, where only those stationary points related to the chemical reaction have been included. This means that only those minima on the PES representing chemically different species, and the saddle points connecting them, have been taken into account in the proposed mechanism. The reaction mechanism can be described as follows: from the reactants, two adducts can be formed, one following the Markownikoff rule, MO; the other, MOp, is formed in a contra-Markownikoff way. From each of the MO and MOp adducts, a pathway is found giving 1,2-epoxypropane, P1, and from this, two ways lead to propanal, P2, and propanone, P2p. Eventually, P2 can react to give 1-propenol, P4, and, from it, 3-propenol, P3, and P2p can give 2-propenol, P4p. Also, from both MO and MOp a pathway is found giving a five-membered cyclic adduct, M2, which breaks in two different ways, giving two alkoxy radicals, P6 and P6p; these eventually break to give formaldehyde and ethanal, P7. Finally, we have found two direct paths connecting MO with P2 and MOp with P2p. The whole reaction mechanism including only the reactants and the different products is shown in Scheme 2.

The B3LYP/6-31G* optimized geometries of the reactants, products, intermediates, and transition states (TS) of this reaction system are depicted in Figures 1 and 2. The energy profile of the reaction is illustrated in Figures 3 and 4, at the B3LYP/6-31G* and CASSCF(7,7)/6-31G* levels, respectively.

3.1.1. Initial Adducts. Recent studies employing MP2/6-31G*, MP2/6-311G**, B3LYP/6-31G*, and B3LYP/6-311G**, as well as other accurate theoretical techniques such as CBS, BAC, G2, and G2(MP2) on the OH + ethene reaction have shown[26] that a van der Waals complex is formed prior to addition. A transition state connecting this van der Waals complex with the adduct has also been found, and its energy is very similar to that of the complex. Similar results have also been obtained on the NO_3 + ethene reaction.[27] In the case of the

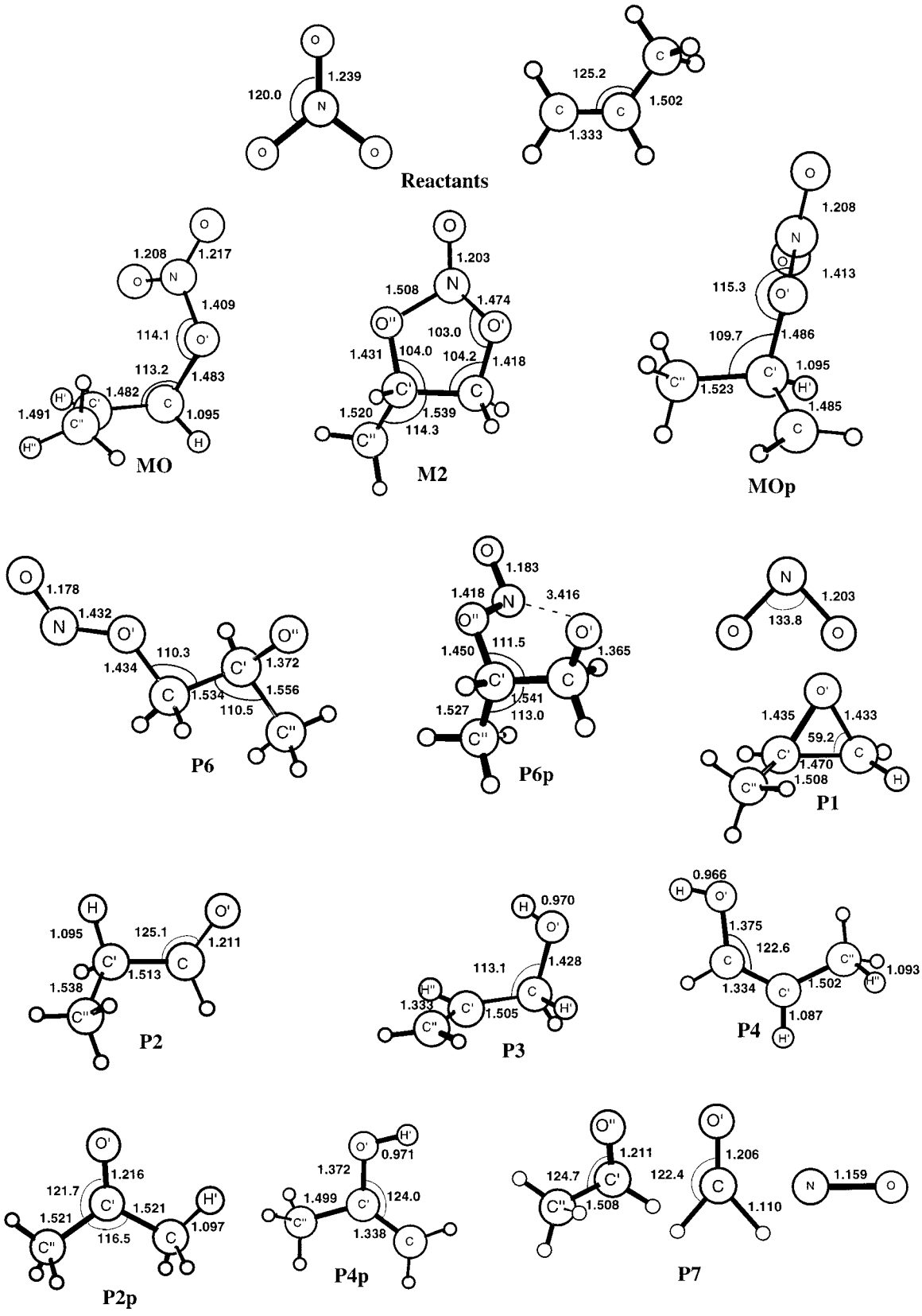

Figure 1. Optimized geometries of reactants, products, and intermediates for the NO_3 + propene addition reaction, at the B3LYP/6-31G* level of theory. Unlabeled atoms correspond to nonrelevant hydrogen atoms.

propene + NO_3 reaction, only the transition state, TScM, leading to a contra-Markownikoff adduct, has been found at the B3LYP/6-31G* level of calculation. Neither the van der Waals complexes (in the Markownikoff and contra-Markownikoff oriented addition reaction paths) nor the transition state previous to the Markownikoff adduct, TSM, have been found at this level of theory and basis set, because they actually represent only small irregularities on the potential energy hypersurface. The van der Waals complexes are not chemically relevant in the reaction mechanism.[28] This is not the case for the transition

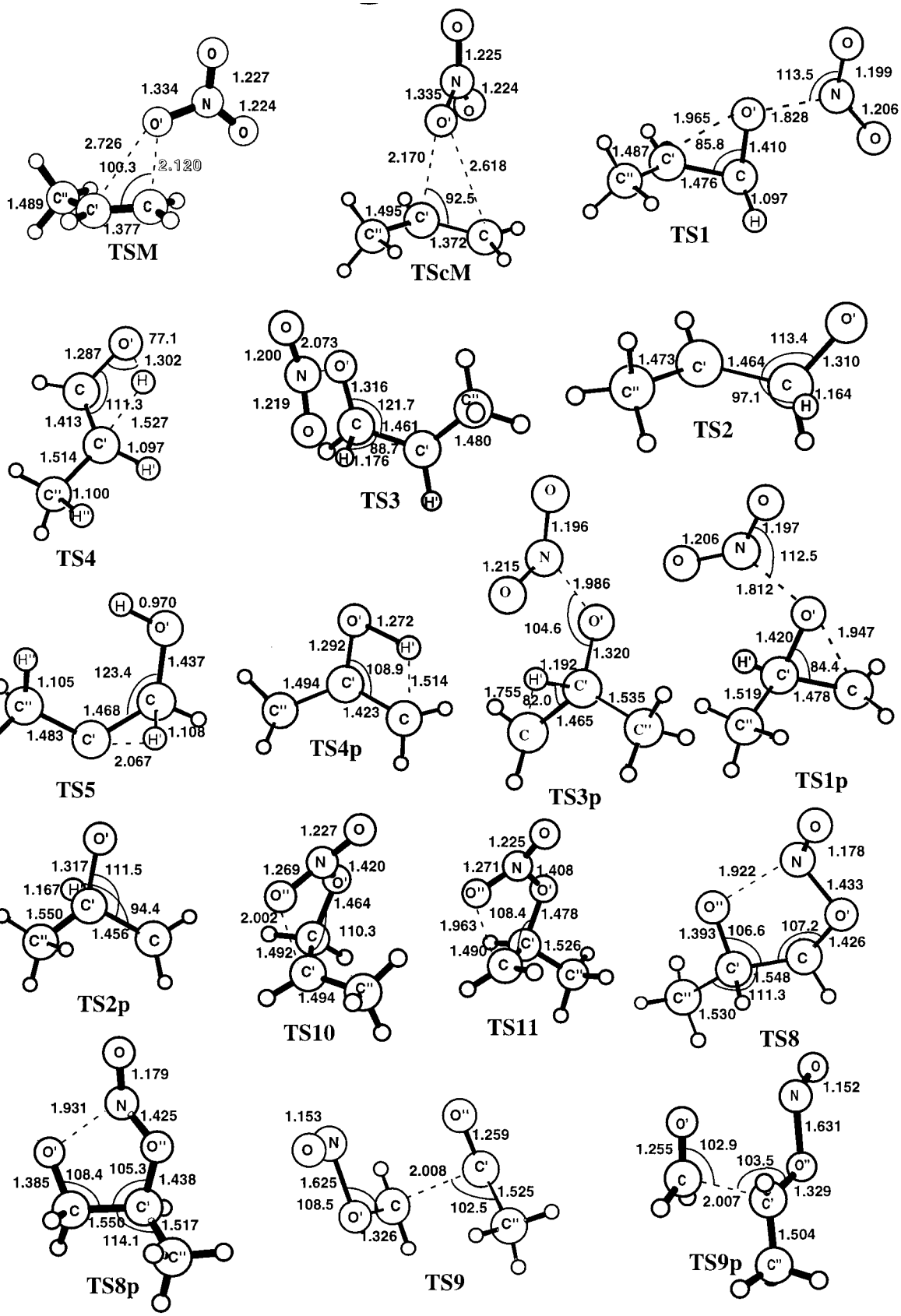

Figure 2. Optimized geometries of transition states for the NO_3 + propene addition reaction, at the B3-LYP/6-31G* level of theory. Unlabeled atoms correspond to nonrelevant hydrogen atoms. Parameters noted for dashed lines correspond to fixed distances.

states connecting the van der Waals complexes with their respective adducts, because the involved barriers control the rate of the disappearance of the reactants, which corresponds to the experimentally measured rate constants.[29]

An estimation of TSM was done by fixing the O′−C distance (see Figure 2) and then by optimizing the rest of the parameters. The energy of the stationary point found by this way, relative to reactants, is −2.38 (−2.15) kcal mol^{-1} (in all cases the first

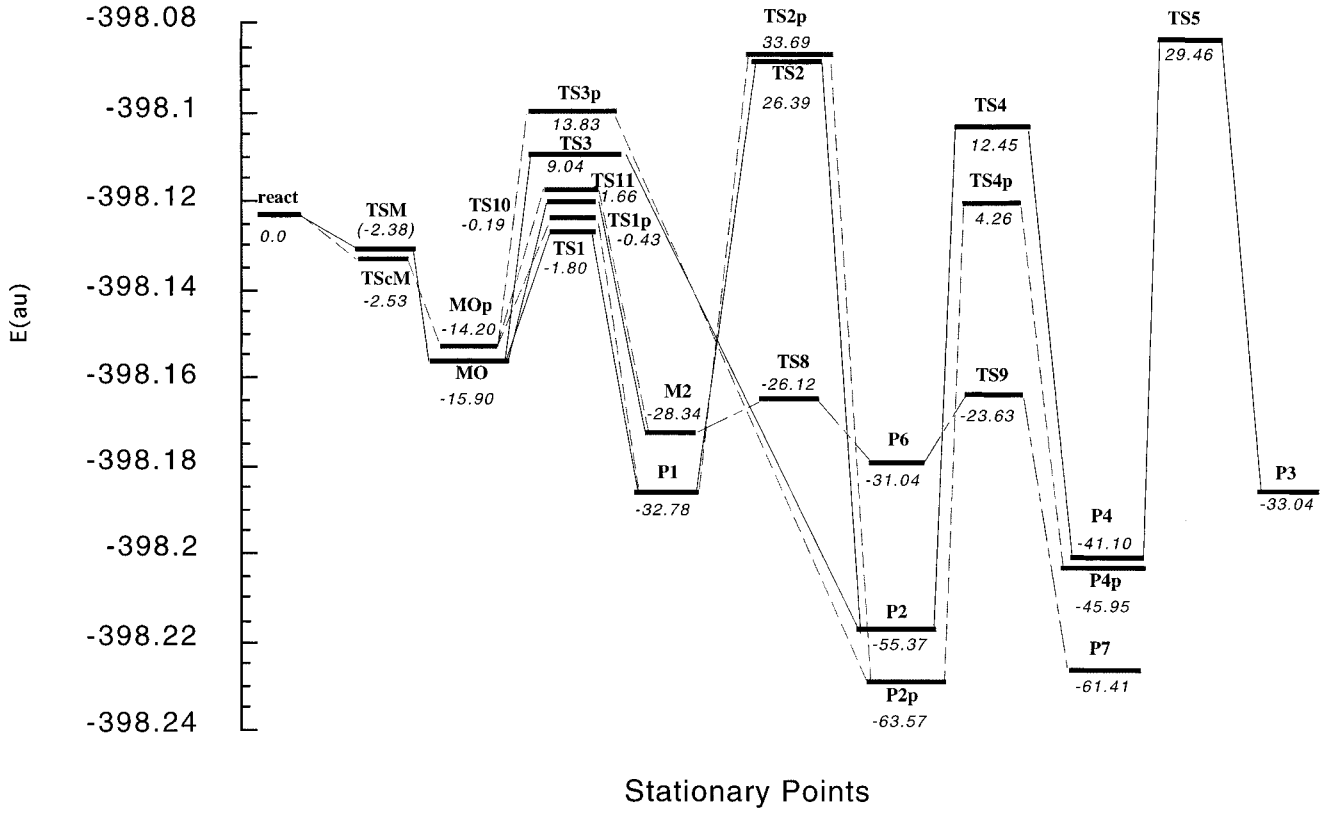

Figure 3. Reaction profile for the addition reaction NO_3 + propene at the B3LYP/6-31G* level of theory. Energies relative to reactants are in kcal mol^{-1}.

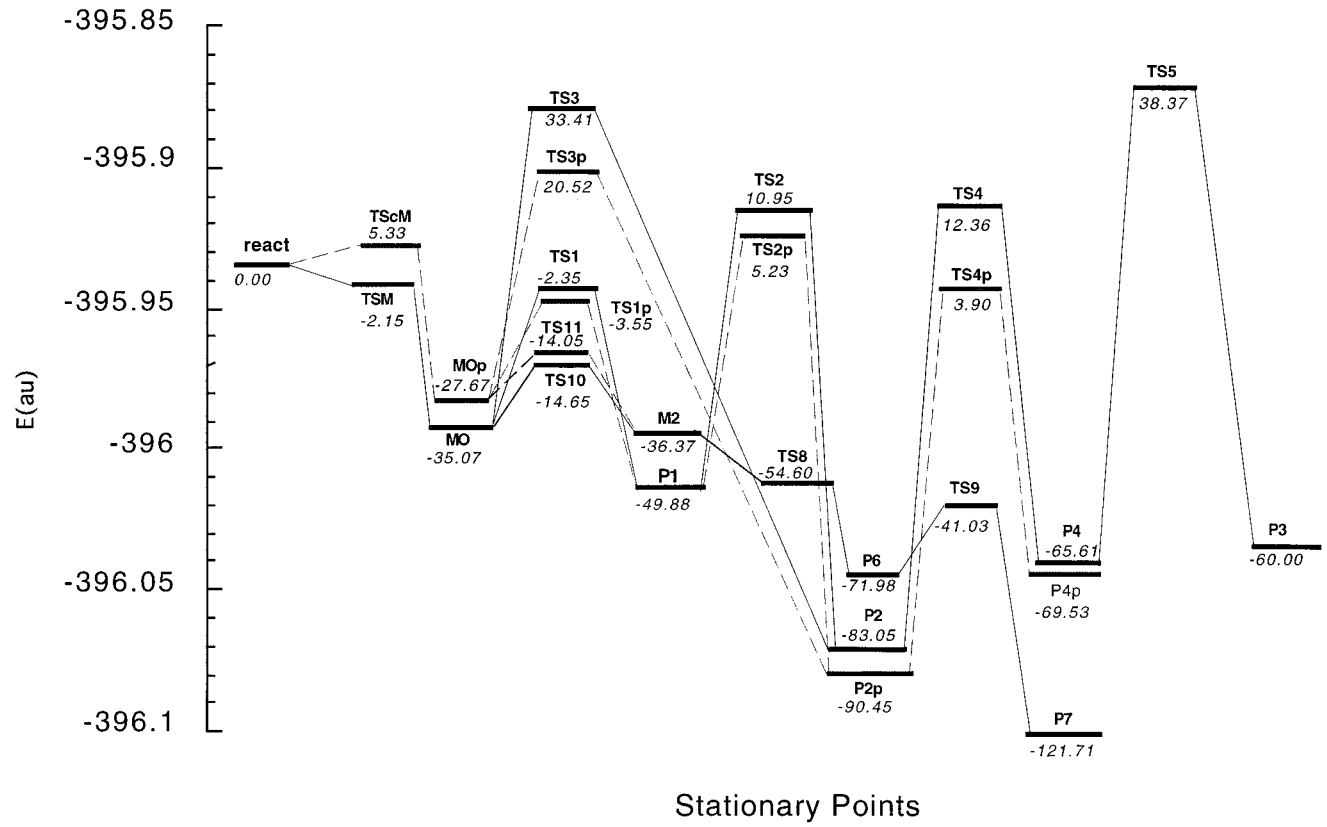

Figure 4. Reaction profile for the addition reaction NO_3 + propene at the CASSCF(7,7)/6-31G* level of theory. Energies relative to reactants are in kcal mol^{-1}.

number refers to the B3LYP/6-31G* result and the second, in parentheses, to the CASSCF(7,7)/6-31G* result). Since the conformation obtained in this way is only an approximation to the true TSM transition state, two imaginary frequencies have been found: the first one, at 243i cm^{-1}, is associated with the symmetric movement of the oxygen O′ toward the carbon C,

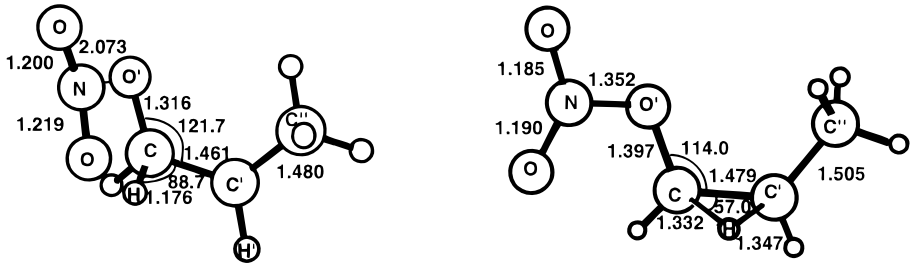

Figure 5. Optimized geometries of the TS3 transition state for the NO_3 + propene addition reaction, at the B3-LYP/6-31G* and CASSCF(7,7)/6-31G* levels of theory. Unlabeled atoms correspond to nonrelevant hydrogen atoms.

and the second one is very small (28i cm^{-1}) and corresponds to a movement associated with the relative orientation of the two fragments and can, therefore, be neglected.

The energy of the MO adduct relative to reactants is −15.90 (−35.07) kcal mol^{-1}. The relationship between B3LYP/6-31G* and CASSCF(7,7)/6-31G* values will be discussed later. This secondary radical adduct is stabilized by the methyl group and also by an hyperconjugative effect of the C−H bonds. The largest negative charge lies on the C″ atom (for the notation see Figures 1 and 2), due to the greater donor character of the methyl group. The spin density is mainly on the C′ atom, as a confirmation of the experimental suggestion that an electrophilic addition to the double bond is taking place.

For the contra-Markownikoff-oriented addition pathway, we have found a stationary point, TScM, at −2.53 (5.33) kcal mol^{-1} leading from the reactants to the MOp adduct. This point has been characterized as a transition state and shows an imaginary frequency of 152i cm^{-1}. The reaction coordinate involved corresponds to the symmetric movement of the oxygen atom toward the more substituted carbon atom on the double bond. In TScM, the NO_3 radical is placed with two oxygen atoms in a bridged conformation on the double bond and lies in a plane perpendicular to the double bond (see Figure 2). The spin density is mainly on the O′ and C atoms; hence, the radical character is localized not only on the NO_3 fragment but also on the π system. The conformation of the propene fragment is the most favorable one, showing the double bond eclipsed.

The energy of the MOp adduct, relative to reactants, is −14.20 (−27.67) kcal mol^{-1}; the spin density is mainly on the C atom, and it is not stabilized by donor groups.

In the presence of oxygen molecules, as actually occurs in the atmosphere, both intermediates, MO and MOp, will be oxidized on the carbon atom which shows the largest spin density (C′ for MO and C for MOp), giving peroxides as products, as is experimentally found.[30]

3.1.2. 1,2-Epoxypropane Formation. The Markownikoff adduct MO reacts through TS1 to P1, and the reaction coordinate involves the closure of the C′−C−O′ angle and the enlargement of the O′−N distance (see Figure 1). Relative to MO, this step is exothermic by 16.88 (14.81) kcal mol^{-1} and involves an energy barrier of 14.00 (32.72) kcal mol^{-1}. However, relative to reactants, TS1 is at −1.80 (−2.35) kcal mol^{-1} and shows an imaginary frequency of 666i cm^{-1}. The spin density is on C′ and N. These results are similar to those found for the NO_3 + ethylene reaction mechanism.[12] P1 (1,2-epoxypropane) and NO_2 are the products experimentally found.[7,8]

Also, the contra-Markownikoff adduct MOp reacts through TS1p to P1. The reaction coordinate involves the closure of the C−C′−O′ angle and the enlargement of the O′−N distance (see Figure 1). Relative to MOp, this path is exothermic by 18.58 (22.21) kcal mol^{-1} and involves an energy barrier of 13.77 (24.12) kcal mol^{-1}. However, TS1p is at −0.43 (−3.55) kcal mol^{-1}, relative to reactants, and shows an imaginary frequency of 698i cm^{-1}.

3.1.3. Propanal, 1-Propenol, and 3-Propenol Formation. 1,2-Epoxypropane (P1) can react through TS2 to P2. The reaction coordinate involves the opening of the three-membered ring, a 1,2-hydrogen transfer from C to C′, and the shortening of the C−O′ bond. Relative to P1, this path involves a significant energy barrier of 59.17 (60.83) kcal mol^{-1}, but the overall reaction is exothermic by 22.59 (33.17) kcal mol^{-1}. The transition state involved, TS2, is at 26.39 (10.95) kcal mol^{-1}, relative to reactants, and shows an imaginary frequency of 705i cm^{-1} associated with the opening of the ring. The energy barrier involved makes this step very unlikely from a kinetic point of view.

We have also found another path which goes directly from MO to P2 through TS3. NO_2 is also formed. The reaction coordinate involves a 1,2-hydrogen transfer from the C to the C′ carbon atom and the enlargement of the O′−N bond. Relative to MO, this step shows an energy barrier of 24.94 (68.48) kcal mol^{-1}, although the whole step is exothermic by 39.47 (47.98) kcal mol^{-1}. The TS3 transition state is at 9.04 (33.41) kcal mol^{-1}, relative to reactants, and shows an imaginary frequency of 536i cm^{-1}, related to the decreasing of the H−C−C′ angle. The large difference between the B3LYP/6-31G* and CASSCF(7,7)/6-31G* values for the TS3 energy can be explained because the geometries obtained at both levels of calculation are somewhat different (see Figure 5). At the B3LYP/6-31G* level, the TS3 transition state shows a rather long O′−N distance, while the 1,2-hydrogen transfer is still in a preliminary stage. However, at the CASSCF(7,7)/6-31G* level, TS3 shows a short O′−N distance and the 1,2-hydrogen transfer has almost taken place. The whole reaction coordinate is the same in both cases, but it is followed in a different order. The spin density in the B3LYP/6-31G* transition state is on the nitrogen and C′ carbon atoms. For the CASSCF(7,7)/6-31G* transition state the spin density is distributed among the two carbon atoms.

P2 reacts through TS4 to P4. The reaction coordinate involves a hydrogen transfer from the CH_2 group to the carbonyl oxygen atom. Relative to P2, there is a huge energy barrier of 67.82 (95.41) kcal mol^{-1}, and this intramolecular path is endothermic by 14.27 (17.44) kcal mol^{-1}. Relative to reactants, the transition state, TS4, connecting the aldehyde P2 and the enol P4, is at 12.45 (12.36) kcal mol^{-1} and shows an imaginary frequency of 2211i cm^{-1}.

From P4, another intramolecular path leads to the 1-propenol formation, P3, through TS5. This path is endothermic by 8.06 (5.61) kcal mol^{-1}, and the energy barrier is very high, 70.56 (104.48) kcal mol^{-1}, both values being relative to P4. Relative to reactants, TS5 is at 29.46 (38.87) kcal mol^{-1} and involves two 1,2-hydrogen transfers, from C′ to C and from C″ to C′, with an associated imaginary frequency of 218i cm^{-1}.

3.1.4. Propanone and 2-Propenol Formation. A reaction coordinate leads from P1 to P2p, through TS 2p, and involves the opening of the ring, a 1,2-hydrogen transfer from the C′ to the C atom, and the shortening of the O′−C′ bond length to form the double bond of the carbonyl group. Relative to P1, the involved energy barrier is very high, 66.38 (55.11) kcal mol^{-1}, although the whole step is exothermic by 30.79 (40.57) kcal mol^{-1}. TS 2p is at 33.69 (5.23) kcal mol^{-1}, relative to reactants, and shows an imaginary frequency of 927i cm^{-1}.

MOp can react directly through TS3p to P2p (propanone), and this step is exothermic by 49.37 (62.78) kcal mol^{-1}, but there is a significant energy barrier of 28.03 (48.19) kcal mol^{-1}. The reaction coordinate involves a 1,2-hydrogen transfer from C′ to C (see Figure 1) and the enlargement of the O′−N bond. The involved transition state, TS3p, has an energy, relative to reactants, of 13.83 (20.52) kcal mol^{-1} and shows an imaginary frequency of 862i cm^{-1}. The spin density is mainly on C and on N.

The next step is an intramolecular reaction which is endothermic by 17.62 (20.92) kcal mol^{-1}, leading from P2p to the enol form, P4p, through TS4p, which represents a very high energy barrier of 67.83 (94.35) kcal mol^{-1}. The reaction coordinate involves a 1,2-hydrogen transfer to the carbonyl group oxygen atom. TS4p shows an imaginary frequency of 2168 cm^{-1} associated with the 1,2-hydrogen transfer, and the height of the energy barrier is 4.26 (3.90) kcal mol^{-1}, relative to reactants.

3.1.5. Cyclic Adduct and Its Fragmentation. Two reaction pathways starting from either Markownikoff or contra-Markownikoff adducts, MO or MOp, have been found, which lead to exothermic products: formaldehyde, ethanal, and NO. Both pathways converge at the same intermediate, the five-membered-ring structure M2 (see Figure 1), which reacts in two different ways, by cleavage of either one or the other N−O bond.

The step from MO through TS10 to M2 is exothermic by 12.44 (1.30) kcal mol^{-1}, and the barrier is 15.71 (20.42) kcal mol^{-1}. On the another hand, MOp reacts exothermically by 14.14 (8.7) kcal mol^{-1} through TS11 to M2, the barrier being 15.86 (13.62) kcal mol^{-1}.

The five-membered-ring structure M2 is slightly distorted due to the presence of the methyl group. Thus, the O′−C and N−O′ distances are slightly shorter than the O″−C′ and N−O″ ones. Also, the C−C distance suggests a slightly long single bond. The spin density is delocalized on the NO_3 system, mainly on the NO group.

The reaction coordinate leading from either MO or MOp to M2 involves the rotation of the O″−C′−C−O′ dihedral angle and the formation of a bond between the oxygen O″ and either the C′ carbon atom (from MO) or the C atom (from MOp; see Figure 2). The two transition states involved, TS10 and TS11, show imaginary frequencies of 675i and 712i cm^{-1}, respectively, and are at −0.19 (−14.65) and 1.66 (−14.05) kcal mol^{-1}, respectively, relative to reactants. Their geometries show that the NO_3 system is placed in such a way that two oxygen atoms form a near-bridging conformation over the C−C bond. The spin density is on the C atom of the CH_2 group and the N and O atoms.

The cleavage of the N−O″ bond in M2 is exothermic by 2.70 (35.61) kcal mol^{-1} and gives the alkoxy radical, P6, through the transition state TS8, with a barrier energy of 2.22 (−18.23) kcal mol^{-1}, whereas the cleavage of the N−O′ bond is exothermic by 1.75 (30.53) kcal mol^{-1} and gives another alkoxy radical, P6p, through TS8p, with a barrier energy of 2.10 (−29.67) kcal mol^{-1}. Even with the perspective of the quantitative differences between CASSCF(7,7)/6-31G* and B3LYP/6-31G* results, the discrepancies between these CASSCF(7,7)/6-31G* and B3LYP/6-31G* values can be interpreted in terms of a poor description of the M2 ring structure at the CASSCF(7,7)/6-31G* level, resulting in a relative energy that is too high, as can be seen after comparing Figures 3 and 4. In P6, the spin density is mainly on the O″ atom, while that in P6p is on O′. P6 is more stable than P6p by 0.95 (5.08) kcal mol^{-1}, since the spin density is stabilized by the methyl group in P6 and not in P6p.

The reaction coordinate from M2 to two nitrite alkoxy radicals, P6 and P6p, can be described in terms of an enlargement of either the N−O″ or N−O′ bond, and a change of the O−N−O″−O′ dihedral angle. The transition state in the reaction coordinate for the N−O″ cleavage, TS8, is at −26.12 (−54.60) kcal mol^{-1} from reactants, and shows an imaginary frequency of 196i cm^{-1}. The spin density is on the NO_3 system and shows the value of the density on O″ atom is double that on the other O atoms. On the other hand, the transition state for the N−O′ bond cleavage, TS8p, is at −26.24 (−66.04) kcal mol^{-1} and shows an imaginary frequency of 210i cm^{-1}.

Homolytic cleavage of the C−C bond in either P6 or P6p gives the final products, P7, formaldehyde, ethanal, and NO, through TS9 or TS9p, respectively. These paths are exothermic by 30.40 (49.73) and 31.32 (54.81) kcal mol^{-1}, and the energy barriers from P6 and P6p are 7.41 (30.96) and 5.73 (29.51) kcal mol^{-1}. The transition vector involves the enlargement of either N−O′ or N−O″ bonds, to form NO, and the shortening of either O″−C′ or O′−C distances, to form the carbonyl group. TS9 is at −23.63 (−41.03) kcal mol^{-1} from reactants, and shows an imaginary frequency of 471i cm^{-1}. The spin density is on C and O″ atoms. TS9p is −24.36 (−37.39) kcal mol^{-1} from the reactants and shows an imaginary frequency of 415i cm^{-1}.

3.2. Comparison of B3LYP/6-31G* and CASSCF(5,6)/6-31G* Geometries. Several stationary points were fully optimized at the CASSCF(5,6)/6-31G* level to calibrate the reliability of DFT using the B3LYP functional and 6-31G* basis set for calculating geometries of the systems involved in this work. B3LYP/6-31G* and CASSCF(5,6)/6-31G* optimized geometries are summarized in Tables 1 and 2.

We have considered five stationary points of the whole potential energy surface: one transition state and four minima, all of them characterized after the Hessian matrix diagonalization.

The average of the absolute values of the differences for angles is 0.8° and for distances is 0.011 Å. The C−C distances are different by less than 0.01 Å in all cases, except for the P1 C′−C distance, where the difference is only 0.014 Å. However, for the C−O distances the agreement is poorer. MO, P1, and TS4 show differences in the 0.20−0.30 Å range, although the errors in C′−O′ distances are related with large values; thus, the relative errors are not significant. Only the C−O′ distances for MO, P1, and TS4 are meaningful. TS3 was also optimized at the CASSCF(5,6)/6.31G* level, but, as has been discussed above, the obtained structure is not equivalent to that found at the B3LYP/6.31G* level and cannot be compared in this way. Nevertheless, deviations of the B3LYP/6-31G* geometries from the CASSCF(5,6)/6-31G* ones are small enough to consider that the B3LYP/6-31G* level of calculation is a good compromise between quality and computational cost for the study of our systems.

3.3. Comparison of CASSCF(7,7)/6-31G* and B3LYP/6-31G* Energy Values. Table 3 shows the B3LYP/6-31G* and CASSCF(7,7)/6-31G* energies, including the zero point energy correction, for the studied stationary points as well as the

TABLE 1: CASSCF(5,6)/6-31G(d) and B3LYP/6-31G(d) Interatomic Distances and Absolute Differences between CASSCF and B3LYP Values, in Å

param	method	MO	P1	P2	P4	TS4
r(C′−C)	CASSCF	1.490	1.456	1.508	1.335	1.412
	B3LYP	1.482	1.470	1.513	1.334	1.413
	Δ	0.008	0.014	0.005	0.001	0.001
r(C″−C′)	CASSCF	1.499	1.504	1.532	1.503	1.514
	B3LYP	1.491	1.508	1.538	1.502	1.514
	Δ	0.008	0.004	0.006	0.001	0.000
r(O′−C)	CASSCF	1.454	1.403	1.206	1.366	1.266
	B3LYP	1.483	1.433	1.211	1.375	1.287
	Δ	0.029	0.030	0.005	0.009	0.021
r(O′−C′)	CASSCF	2.455	1.448	2.403	2.367	2.205
	B3LYP	2.476	1.435	2.421	2.377	2.230
	Δ	0.021	0.011	0.018	0.010	0.025

TABLE 2: CASSCF(5,6)/6-31G(d) and B3LYP/6-31G(d) Angles and Dihedral Angles and Absolute Differences between CASSCF and B3LYP Values, in Degrees

param	method	MO	P1	P2	P4	TS4
∠(C−C′−C″)	CASSCF	120.3	122.5	111.9	125.5	123.5
	B3LYP	121.6	122.4	111.9	125.2	124.8
	Δ	1.3	0.1	0.0	0.3	1.3
∠(O′−C−C′)	CASSCF	117.6	117.4	108.0	116.7	109.4
	B3LYP	118.1	117.2	108.4	116.6	110.2
	Δ	0.5	0.2	0.4	0.1	0.8
∠(O′−C−C′)	CASSCF	113.0	60.8	124.2	122.4	110.7
	B3LYP	113.2	59.2	125.1	122.6	111.3
	Δ	0.2	1.6	0.9	0.2	0.6
∠(O′−C−C′−C″)	CASSCF	−65.9	−102.8	−125.8	1.4	153.6
	B3LYP	−70.3	−103.8	−126.5	0.0	153.2
	Δ	4.4	1.0	0.7	1.4	0.4

experimental enthalpies of formation for the products. The relative energies relative to propene + NO_3 for each stationary point are included in Table 3 along with experimental enthalpies of reaction. Values for differences between energies of meaningful stationary points on the PES are presented in Table 4. B3LYP/6-31G* and CASSCF(7,7)/6-31G* reaction profiles are then depicted in Figures 3 and 4 from the values in Table 3.

Comparison between the experimental enthalpies of reaction and theoretical values show that the B3LYP/6-31G* calculations reproduce the experimental values within 5 kcal mol^{-1} except for propenol (P3). B3LYP/6-31G* seems thus to be more reliable than CASSCF(7,7)/6-31G* with the selected active space in reproducing the enthalpies of the products. Since we do not have information on the experimental transition state energies, we cannot evaluate the accuracy of theoretical methods in these stationary points.

3.4. Reaction Analysis. The Markownikoff radical adduct, MO, is calculated to be more stable than the contra-Markownikoff radical adduct, MOp, by 1.70 kcal mol^{-1}, due to the hyperconjugation stabilization of the CH_3 donor group. The high stabilization energy of the initial radical adduct (15.90 kcal mol^{-1}) makes its formation in the troposphere probable.

At the B3LYP/6-31G* level, the transition state TScM leading from the reactants to the contra-Markownikoff radical adduct, MOp, is 2.53 kcal mol^{-1} lower than the reactants. However, at the CASSCF(7,7)/6-31G* level, this transition state is 5.33 kcal mol^{-1} higher than the reactants. Both levels of theory show a transition state, TSM, 2.38 (2.15) kcal mol^{-1} lower than the reactants for the reaction step leading from reactants to the Markownikoff radical adduct, MO. The B3LYP/6-31G* estimated transition state (TSM) enthalpy leading from the reactants to the Markownikoff radical adduct, MO, is slightly higher (0.15 kcal mol^{-1}) than the contra-Markownikoff transition state, TScM. This apparently anomalous result can be explained because the Markownikoff transition state is not completely optimized but estimated, as it has been previously pointed out. In any case, transition states with energy lower than the reactants are frequently found in radical addition reactions and are frequently explained by the presence of a previous van der Waals complex between the reactants.[31,32]

In both the B3LYP/6-31G* and CASSCF(7,7)/6-31G* reaction profiles, the transition states TS1 and TS1p, leading to 1,2-epoxypropane + NO_2 (P1), and TS10 and TS11, leading to formaldehyde, ethanal, and NO (P7), are lower than the initial energy of reactants, except for TS11 at the B3LYP/6-31G* level, although in this case its value is small (1.66 kcal mol^{-1}). Thus, since the reactants enter in the reaction channel at an energy higher than these barriers, we can expect that all these products will be directly accessible in the reaction channel. In other words, one can think that the energy evolved in the formation of the MO adduct is large enough to allow MO to overcome *both* barriers, TS1 and TS10. Further deactivation of all the obtained products will produce an equilibrium distribution between the radical adduct and the 1,2-epoxypropane and the NO_2 (P1), which are the products experimentally found by Wille et al.[7,8] and the formaldehyde, ethanal, and NO (P7), which are the products experimentally found by Bandow et al.[33] If the reaction occurs in the presence of oxygen molecules, the oxidization of the radical adduct will give peroxides, according to the experimental observations.[10,11] 1,2-Epoxypropane (P1) and the Markownikoff radical adduct, MO, are thermodynamically less stable than ethanal, formaldehyde, and NO (P7), and the latter will be therefore the main products, the former being produced in a minor proportion.

In the B3LYP/6-31G* and CASSCF(7,7)/6-31G* reaction profiles, formaldehyde, ethanal, NO (P7) and propanone (P2) are the most stable products from the thermodynamic point of view, and they would be the main products if the reaction control was thermodynamic. The height of the barrier leading to propanone is very different at the two levels of calculation. At the B3LYP/6-31G* level the barrier involved is 9.04 kcal mol^{-1}; therefore, the ketone formation would be possible at high temperatures. In constrast, at the CASSCF(7,7)/6-31G* level, the barrier involved is 33.41 kcal mol^{-1}; thus, this high barrier makes the propanone formation very unlikely in the atmospheric chemistry.

The energy value, relative to reactants, corresponding to the transition states leading to the Markownikoff and contra-Markownikoff radical adducts is −2.38 kcal mol^{-1} at the B3LYP/6-31G* level and −2.15 kcal mol^{-1} at the CASSCF(7,7)/6-31G* level. The experimental activation energy, E_a, is around 2.32 kcal mol^{-1}, [29,34] which is also the estimated value using frontier orbital theory.[35] Since the experimental values for the activation energy have a reliability range of around 30%,[29] and the estimated confidence margin for the theoretical calculations is 0.5 eV, we can conclude that the calculations are within the range of the experimental values. Thus, the B3LYP/6-31G* mechanism can be assumed to be in agreement with the experimental studies on this point. Therefore, B3LYP/6-31G* calculations seem to be more reliable than CASSCF(7,7)/6-31G* ones, since in the latter case it is very difficult to define an active space coherent all along the potential energy hypersurface.

4. Conclusions

A theoretical study of the addition reaction of the nitrate radical to propene including geometry optimization and char-

TABLE 3: B3LYP/6-31G(d) Total Energies of Formation and CASSCF(7,7)/6-31G(d) Total Energies in au and Enthalpies of Formation in kcal mol^{-1}

stationary point	B3LYP	CASSCF	ΔH_f^{o} [36]	B3LYP[a]	CASSCF[a]	ΔH_r^{o} [a]
propene + NO_3	−398.124 354	−395.933 425	22.42	0.00	0.00	0.0
TSM	(−398.132 270)	−395.940 984		(−2.38)	−2.15	
TScM	−398.132 639	−395.929 127		−2.53	5.33	
MO	−398.156 085	−395.995 627		−15.90	−35.07	
TS1	−398.131 071	−395.942 017		−1.80	−2.35	
P1	−398.180 722	−396.017 759	−14.48	−32.78	−49.88	−36.9
TS2	−398.079 050	−395.912 828		26.39	10.95	
TS3	−398.109 397	−395.881 651		9.04	33.41	
P2	−398.215 638	−396.069 831	−36.22	−55.37	−83.05	−58.64
TS4	−398.101 453	−395.911 543		12.45	12.36	
P4	−398.192 877	−396.041 859		−41.10	−65.61	
TS5	−398.075 960	−395.870 014		29.46	38.87	
P3	−398.180 254	−396.033 422	−21.60	−33.04	−60.00	−44.02
MOp	−398.152 543	−395.983 021		−14.20	−27.67	
TS1p	−398.128 771	−395.942 750		−0.43	−3.55	
TS2p	−398.068 250	−395.922 123		33.69	5.23	
TS3p	−398.101 832	−395.900 176		13.83	20.52	
P2p	−398.227 898	−396.080 997	−43.81	−63.57	−90.45	−63.23
TS4p	−398.114 352	−395.924 950		4.26	3.90	
P4p	−398.200 733	−396.048 112		−45.95	−69.53	
TS10	−398.130 598	−395.962 713		−0.19	−14.65	
TS11	−398.127 660	−395.961 781		1.66	−14.05	
M2	−398.178 382	−396.000 178		−28.34	−36.37	
TS8	−398.173 154	−396.027 553		−26.12	−54.60	
TS8p	−398.173 233	−396.045 736		−26.24	−66.04	
P6	−398.179 846	−396.054 097		−31.04	−71.98	
P6p	−398.177 300	−396.045 031		−30.09	−66.90	
TS9	−398.164 164	−396.000 891		−23.63	−41.03	
TS9p	−398.165 303	−395.995 132		−24.36	−37.39	
P7	−398.218 746	−396.125 778	−43.91	−61.41	−121.71	−66.33

[a] Energies relative to the reactant in kcal mol^{-1}. Zero point corrections have been included in B3LYP/6-31G* and CASSCF(7,7)/6-31G* energy differences. The values in parentheses correspond to an estimated point. Theoretical and experimental enthalpy values are taken at 298.15 K.

TABLE 4: Energy Differences in kcal mol^{-1} for the NO_3 + Propene Reaction[a]

	B3LYP	CASSCF	exptl[1]
TSM−reactants	(−2.38)	−2.15	2.32
TScM−reactants	−2.53	5.33	2.32
TS1−reactants	−1.80	−2.35	
TS1p−reactants	−0.43	−3.55	
TS3−reactants	9.04	33.41	
TS3p−reactants	13.83	20.52	
MO−reactants	−15.90	−35.07	
MOp−reactants	−14.20	−27.67	
TS1p−TSO	2.10	−8.89	
TS1−TS1p	−1.37	1.20	
TS1−MO	14.10	32.72	
TS1p−MOp	13.77	24.12	
MO−MOp	−1.70	−7.40	
TS2−P1	54.17	60.83	
TS3−MO	24.94	68.48	
TS3p−MOp	28.03	48.19	
TS2p−P1	66.47	55.11	
TS4−P2	67.82	95.40	
TS4p−P2p	67.83	94.34	
TS5−P4	70.56	104.45	
TS2−TS1	28.19	13.30	
TS2p−TS1p	34.12	8.78	
TS4−TS3	3.41	−21.05	
TS3−TS1	10.84	35.77	
TS3p−TS1p	14.26	24.07	
TS10−reactives	−0.19	−14.65	
TS11−reactives	1.66	−14.05	
M2−reactives	−28.34	−36.37	
TS10−TS1	1.61	−12.85	
TS11−TS1	3.46	−12.25	
TS11−TS10	1.85	0.60	

[a] Zero point correction has been included.

acterization of the stationary points at density functional theory using the B3LYP functional and the 6-31G* basis set has been carried out. The energy values have been also calculated at B3LYP/6-31G* geometries with CASSCF/6-31G* level including seven active electrons in seven active orbitals. Two main reaction pathways, resulting from the Markownikoff and contra-Markownikoff addition on the double bond of the NO_3 radical, have been identified. Two initial transition states lead to the Markownikoff and contra-Markownikoff addition, with energies lower than the reactant energy. Different products have been identified, in pathways starting from the same intermediate, which can be identified with the adduct suggested experimentally.[1] The products found in the Markownikoff addition are: epoxide, aldehyde, ketone and its enol, formaldehyde, ethanal, and NO.

Taking into account experimental data and the mechanism proposed in this work we can conclude that, at low pressures and temperatures, an equilibrium distribution is produced between 1,2-epoxypropane, the NO_2, the radical adduct, formaldehyde, ethanal, and NO. Since the last three compounds are thermodynamically more stable than the others, they will be the main products.

At higher temperatures, for instance in combustion processes, the system could have enough energy to overcome the barrier to form ketone. Therefore, a minor quantity of ketone could be formed, but this pathway will be less important. This mechanism would be in agreement with Wille et al.,[7,8] Berndt et al.,[11] and Bandow et al.,[6] who proposed a mechanism where the formation of formaldehyde and ethanal occurs if O_2 is added after NO_3 addition to the double bond. In our proposed mechanism there is a reaction pathway leading to the same products, but in the absence of oxygen.

Acknowledgment. M.P.P.-C. thanks the Ministerio de Educación y Ciencia for a personal grant. This work was supported by the Spanish DGICYT (Projects PB97-1381 and PB97-1383).

References and Notes

(1) Wayne, R. P.; Barnes, I.; Biggs, P.; Burrows, J. P.; Canosa-Mas, C. E.; Hjorth, J.; Bras, G. L.; Moortgat, G. K.; Perner, D.; Poulet, G.; Restelli, G.; Sidebottom, H. *Atmos. Environ.* **1991**, *25A*, 1.

(2) Atkinson, R. *J. Phys. Chem. Ref. Data* **1991**, *20*, 459.

(3) Atkinson, R.; Aschmann, S. M.; J. N. Pitts, J. *J. Phys. Chem.* **1988**, *92*, 3454.

(4) Morris, E. D. J.; Niki, H. *J. Phys. Chem.* **1974**, *78*, 1337.

(5) Japar, S. M.; Niki, H. *J. Phys. Chem.* **1975**, *79*, 1629.

(6) Bandow, H.; Okuda, M.; Akimoto, H. *J. Phys. Chem.* **1980**, *84*, 3604.

(7) Wille, U.; Rahman, M. M.; Schindler, R. N. *Ber. Bunsen-Ges. Phys. Chem.* **1992**, *96*, 833.

(8) Wille, U.; Schindler, R. N. *Ber. Bunsen-Ges. Phys. Chem.* **1993**, *97*, 1447.

(9) Benter, T.; Liesner, M.; Schindler, R. N.; Skov, H.; Hjorth, J.; Restelli, G. *J. Phys. Chem.* **1994**, *98*, 10492.

(10) Berndt, T.; Bøge, O. *Ber. Bunsen-Ges. Phys. Chem.* **1994**, *98*, 869.

(11) Berndt, T.; Bøge, O. *J. Atmos. Chem.* **1995**, *21*, 275.

(12) Pérez-Casany, M. P.; Nebot-Gil, I.; Sánchez-Marín, J.; Tomás-Vert, F.; Martínez-Ataz, E.; as Galán, B.; Aranda-Rubio, A. *J. Org. Chem.* **1998**, *63*, 6978.

(13) Dewar, M. J. S.; Zoebisch, E. G.; Healy, F.; Stewart, J. J. P. *J. Am. Chem. Soc.* **1985**, *107*, 3902.

(14) Slater, J. C. *Quantum Theory of Molecules Solids*; McGraw-Hill: New York, 1974, Vol. 4.

(15) Fock, V. *Z. Phys.* **1930**, *61*, 126.

(16) Becke, A. D. *Phys. Rev.* **1988**, *A38*, 3098.

(17) Vosko, S. H.; Wilk, L.; Nusair, M. *J. Chem. Phys.* **1987**, *87*, 5968.

(18) Lee, C.; Yang, W.; Parr, R. G. *Phys. Rev.* **1988**, *B37*, 785.

(19) Baker, J. *J. Comput. Chem.* **1986**, *7*, 385.

(20) Schlegel, H. B. *J. Comput. Chem.* **1982**, *3*, 214.

(21) Hehre, W. J.; Radom, L.; Schleyer, P. v. R.; Pople, J. A. *Ab initio Molecular Orbital Theory*; Wiley-Interscience: New York, 1986.

(22) Hariharan, P.; Pople, J. *Chem. Phys. Lett.* **1972**, *16*, 217.

(23) Anglada, J.; Bofill, J. *Chem. Phys. Lett.* **1995**, *243*, 151.

(24) Andersson, K.; Fülscher, M.; Karlstrom, G.; Lindh, R.; Malmqvist, P.-A.; Olsen, J.; Roos, B. O.; Sadlej, A. J.; Blomberg, M. R. A.; Siegbahn, P. E. M.; Kello, V.; Noga, J.; Urban, M.; Widmark, P.-O. MOLCAS, version 3; Technical Report; Department of Theoretical Chemistry, Chemical Center, University of Lund, P.O. Box 124, S-221 00 Lund, Sweden, 1994.

(25) Frisch, M. J.; Trucks, G. W.; Schlegel, H. B.; Gill, P. M. W.; Johnson, B. G.; Robb, M. A.; Cheeseman, J. R.; Keith, T.; Petersson, G. A.; Montgomery, J. A.; Raghavachari, K.; Al-Laham, M. A.; Zakrzewski, V. G.; Ortiz, J. V.; Foresman, J. B.; Cioslowski, J.; Stefanov, B. B.; Nanayakkara, A.; Challacombe, M.; Peng, C. Y.; Ayala, P. Y.; Chen, W.; Wong, M. W.; Andres, J. L.; Replogle, E. S.; Gomperts, R.; Martin, R. L.; Fox, D. J.; Binkley, J. S.; Defrees, D. J.; Baker, J.; Stewart, J. P.; Head-Gordon, M.; Gonzalez, C.; Pople, J. A. GAUSSIAN 94, revision d.3; Gaussian Inc., Pittsburgh, PA, 1995.

(26) Piqueras, M.; Crespo, R.; Nebot-Gil, I.; Tomás, F. Manuscript in preparation.

(27) Pérez-Casany, M.; Crespo, R.; Nebot-Gil, I.; Sánchez-Marín, J. Manuscript in preparation.

(28) García-Cruz, I.; Ruiz-Santoyo, M.; Alvarez-Idaboy, J.; Vivier-Bunge, A. *J. Comput. Chem.* **1999**, *20*, 845.

(29) Atkinson, R.; Baulch, D.; Cox, R.; Hampson, R.; Kerr, J.; Ross, M.; Troe, J. *J. Phys. Chem. Ref. Data* **1997**, *26*, 521.

(30) Barnes, I.; Bastian, V.; Becker, K. H.; Tong, Z. *J. Phys. Chem.* **1990**, *94*, 2413.

(31) Singleton, D.; Cvetovic, R. J. *J. Am. Chem. Soc.* **1976**, *98*, 6812.

(32) Mozurkewich, M.; Benson, S. *J. Phys. Chem.* **1984**, *88*, 6429.

(33) Andersson, Y.; Ljungström, E. *Atmos. Environ.* **1989**, *23*, 1153.

(34) Canosa-Mas, C.; Smith, S.; Waywood, S.; Wayne, R. *J. Chem. Soc., Faraday Trans.* **1991**, *87*, 3473.

(35) Marston, G.; Monks, P.; Canosa-Mas, C.; Wayne, R. P. *J. Chem. Soc., Faraday Trans.* **1993**, *89*, 3899.

(36) Lide, D. R. *Handbook of Chemistry and Physics*; CRC Press: Boca Raton, FL, 1996.